ELSEVIER

Contents lists available at ScienceDirect

# Science Bulletin

journal homepage: www.elsevier.com/locate/scib



# Article

# Tumor microenvironment-responsive docetaxel-loaded micelle combats metastatic breast cancer

Tianqun Lang <sup>a,b,1</sup>, Xinyue Dong <sup>a,c,1</sup>, Zhong Zheng <sup>a,d</sup>, Yiran Liu <sup>a,c</sup>, Guanru Wang <sup>a,b</sup>, Qi Yin <sup>a,b,\*</sup>, Yaping Li <sup>a,b,e,\*</sup>

- a State Key Laboratory of Drug Research & Center of Pharmaceutics, Shanghai Institute of Materia Medica, Chinese Academy of Sciences, Shanghai 201203, China
- <sup>b</sup> School of Pharmacy, University of Chinese Academy of Sciences, Beijing 100049, China
- <sup>c</sup>Nano Science and Technology Institute, University of Science and Technology of China, Suzhou 215123, China
- <sup>d</sup> College of Life Sciences, Jilin University, Changchun 130012, China
- <sup>e</sup> School of Pharmacy, Yantai University, Yantai 264005, China

#### ARTICLE INFO

# Article history: Received 26 October 2018 Received in revised form 5 December 2018 Accepted 14 December 2018 Available online 30 December 2018

Keywords: Breast cancer Dual-sensitive micelle Metastasis Tumor-targeting

#### ABSTRACT

Efficient tumor-targeting drug delivery systems are urgently needed for treating metastatic breast cancer. In this work, a docetaxel (DTX)-loaded micelle (pDM) as the tumor-microenvironment-responsive delivery platform is developed. The micelle is composed of a pH-sensitive amphiphilic copolymer, poly((1,4-butanediol)-diacrylate- $\beta$ -N,N-diisopropylethylenediamine)-polyethyleneimine (BD-PEI), and a matrix metalloproteinase (MMP)-responsive polymer, poly((1,4-butanediol)-diacrylate- $\beta$ -N,N-diisopropy lethylenediamine)-peptide-polyethylene glycol (PEG) (BD-peptide-PEG). The PEG block of BD-peptide-PEG will be split by MMPs at the tumor microenvironment, which leads to the change of the surface charge and particle size of the micelle to more positive and smaller one. Owing to this transformation and enhanced permeability and retention (EPR) effect, pDM delivers more DTX into tumor tissues and is internalized more efficiently by tumor cells than the non-MMP-sensitive micelles in the 4T1 tumorbearing mice model. In addition, DTX is released in acidic endo/lysosomes due to the dissociation of the micelle, triggered by the protonation of the hydrophobic block of BD-PEI. As a result, the DTX-loaded micelle inhibits primary tumor growth and pulmonary metastasis effectively. Thus, this pH/MMP-dual-sensitive drug delivery system, which simultaneously attains three keypoints: prolonged circulation time, directional and efficient uptake into tumor cells, and speedy intracellular drug release, is a promising strategy for metastatic breast cancer therapy.

© 2018 Science China Press. Published by Elsevier B.V. and Science China Press. All rights reserved.

# 1. Introduction

Breast cancer is a serious threat to women's health, with the morbidity of 25% and mortality of 15% in female patients [1]. Surgery ablation can control the development of breast cancer at early disease stage [2], but can not destroy distal metastasis [3]. As a result, chemotherapy following surgery is still the preferred clinical treatment option for metastatic breast cancer [4]. Unfortunately, owing to lack of tumor-targeting capacity, the severe side effects of traditional chemotherapy lead to unexpectable pain of patients rather than mitigation [5,6]. What is worse, the long-term administration of chemotherapeutic drugs may induce multidrug resistance and metastasis sites formation [7]. Thus,

E-mail addresses: qyin@simm.ac.cn (Q, Yin), ypli@simm.ac.cn (Y, Li).

developing tumor-targeting drug delivery systems is urgently needed for efficient treatment of metastatic breast cancer.

As cancer therapy is faced with these obstacles, medicine based on nanotechnology is emerging at the right moment [8,9]. The nanomedicine in forms of nanoparticles, liposomes, micelles, and nanoclusters, etc. can passively or actively accumulate in tumor sites, depending on the enhanced permeability and retention (EPR) effects of solid tumors and ligands/antibodies-receptors interactions on the surface of targeted cells [10–12]. To enhance the targeting capacity, the particle sizes, zeta potential and surface properties of nanoparticles are always adjusted to attain the best outcome [13,14]. It has been proved that nanoparticles with better tumor-targeting capacity need to own three characteristics: particles size of 10–100 nm, surface charge close to neutral, and a polyethylene glycol (PEG) coating shell [15]. Paradoxically, nanoparticles with more positive surface charges have higher affinity towards cell membranes, while PEG will screen the

<sup>\*</sup> Corresponding authors.

<sup>&</sup>lt;sup>1</sup> These authors contributed equally to this work.

charges, which hinders their cellular uptake into tumor cells [16,17]. Meanwhile, ensuring sufficient intracellular drug release is another keypoint [18,19]. As a result, circulation time, the uptake efficiency by cells, and drug release rate should be all taken into account to improve the anti-tumor effect of nanoparticles.

To solve the three keypoints mentioned above, various stimuliresponsive nanoparticles have been designed and constructed [20– 23]. Utilizing the special microenvironment of the tumors, the PEG coating can be taken off in response of the condition change at required sites [24]. Metastatic tumor tissues always overexpress matrix metalloproteinases (MMPs) [25]. The peptide, Pro-Leu-Gly-Leu-Ala-Gly (PLG), can be recognized and digested by MMP-9, a main subtype of MMPs. Therefore, introducing a PLG linkage is a good choice to control the leaving of PEG. Moreover, sufficient drug release can be realized by triggering the disruption of the carriers in response to the specific intracellular pH or redox conditions [26,27].

For treatment of metastatic of breast cancer, in this work, a new pH and MMP dual-sensitive micelle as the DTX delivery platform was designed and established. First, the pH-sensitive amphiphilic copolymer, poly((1,4-butanediol)-diacrylate-β-N,N-diisopropyle thyl-enediamine)-polyethyleneimine (BD-PEI) and the MMPresponsive polymer poly((1,4-butanediol)-diacrylate-β-N,N-diiso propylethylenediamine)-PLG-PEG (BD-PLG-PEG) were synthesized. Then BD-PEI, BD-PLG-PEG, and DTX formed a hybrid micelle (pDM). pDM contained a PEG coating on its surface in the circulation, while would lose it owing to the enzymatic cleavage of PLG when met with MMP-9 at tumor tissues. The taking off of PEG caused the increase of zeta potential, which could improve the accumulation of micelles in tumor cells [28]. Because the hydrophobic block BD could be protonated in endo/lysosomes quickly and converted into hydrophilic, pDM dissociated and released DTX quickly upon internalization. The stimulation responsibility, cellular uptake and cytotoxicity in 4T1 cells of pDM were studied. The biodistribution and inhibition effect on tumor growthe and metastasis in the 4T1 lung metastasis mice model were investigated, pDM was expected to simultaneously improve tumor-targeting ability and release DTX timely so as to gain better anti-cancer effect.

# 2. Experimental

#### 2.1. Chemicals and materials

The 6-aminocaproic acid (ACP) modified PLG was synthesized by the GL Biochem Co., Ltd. (Shanghai, China). Methoxypolyethylene glycol<sub>5000</sub>-NH<sub>2</sub> (mPEG-NH<sub>2</sub>) was purchased from Jen-Technology Co. Ltd (Beijing, China). Diisopropylethylenediamine (DPA), 1,4-butanediol diacrylate (BAB), and polyethyleneimine 2000 Da branched (PEI<sub>2000</sub>) were obtained from J&K Scientific Ltd. (Shanghai). RPMI 1640 medium, fetal bovine serum (FBS), active matrix MMP-9, coumarin-6 (C6), Hoechst 33342, LysoTracker Red DND-99 (LysoTracker Red), and 1,1'-dioctadecyl-3,3,3',3'-tetramethylindotricarbocyanine iodide (DiR) were purchased from Thermo Fisher Scientific (Waltham, USA). DTX and dialysis bags were purchased from Meilun Biotech Co., Ltd., (Dalian, China). All other reagents were purchased from Sinopharm Chemical Reagent Co. Ltd and of analytical grade.

#### 2.2. Cell culture

The murine mammary carcinoma cell line 4 T1 was purchased from Cell Bank of Shanghai, Chinese Academy of Sciences (Shanghai). 4 T1 cells were cultured in RPMI (Rosewell Park Memorial Institute) 1640 medium containing 10% FBS, 2.5 g L<sup>-1</sup> glucose,

 $0.11 \text{ g L}^{-1}$  sodium pyruvate, and  $2 \text{ g L}^{-1}$  sodium bicarbonate and maintained at a humidified atmosphere containing 5% CO<sub>2</sub> at 37 °C.

#### 2.3. Animals

Five to six weeks female Balb/c nude mice (18–20 g) were purchased from Shanghai Experimental Animal Center (Shanghai) and fed in the SPF grade environment at the Animal Care Facility. All the experiments that applied animals were conducted under the guideline approved by the Institutional Animal Care and Use Committee (IACUC) of the Shanghai Institute of Materia Medica, Chinese Academy of Sciences.

#### 2.4. Synthesis and characterization of polymers

BD-PEI and BD-PEG were synthesized by Michael addition reaction. First, DPA (1.92 g) was added to BAB (4.00 g) and stirred in the dark for 24 h at 60 °C. The intermediate (BAB-DPA, BD) was dialyzed (molecular weight cut off (MWCO) 3.5 kDa) in ethanol and the solvent was removed by the rotary evaporator (Buchi, Switzerland) 48 h later. Second, BD (0.80 g) was dissolved in dimethyl sulfoxide (DMSO) and PEI<sub>2000</sub> (0.06 g) or mPEG-NH<sub>2</sub> (0.48 g) was added, respectively. The reaction system was stirred at 60 °C for 24 h in dark. The final products BD-PEI and BD-PEG were purified by dialysis (MWCO 3.5 kDa) in water for 24 h and was lyophilized to obtain white powder.

BD-PLG was synthesized according to the following process: ACP-PLG (2 g), anhydrous triethylamine (6 mL), and anhydrous pyridine (6 mL) were mixed together and dissolved in DMSO ahead of time. Then the mixture was added into BD (600 mg) in DMSO, followed by magnetic stirring overnight. The excess of peptides was removed by dialysis (MWCO 1 kDa) against DMSO. BD-PLG was further activated with a ten-fold molar excess of 1hydroxybenzotriazole (HOBT)/1-ethyl-3-(3-dimethylaminopropyl) carbodiimide hydrochloride (EDCI)/N,N-diisopropylethylamine (DIPEA) (1:1:2, molar ratio) in DMSO solution for 4 h. BD-PLG-PEG was synthesized by the reaction between the activated BD-PLG and mPEG-NH<sub>2</sub> under nitrogen protection at room temperature for 24 h, and the excess HOBT, EDCI and DIPEA were removed by dialysis (MWCO 1 kDa) against DMSO for 24 h. After reaction, the product in DMSO was added dropwise to water with five times volume, and then dialyzed in a dialysis bag (MWCO 8 kDa) for 48 h to remove the unreacted PEG. The final product BD-PLG-PEG was lyophilized and stored at -80 °C until use.

The structures of BD, BD-PEI, BD-PEG and BD-PLG-PEG were confirmed by <sup>1</sup>H NMR spectra (Bruker, 400 MHz, Germany), and their molecular weights were tested by MALDI-TOF mass spectrometer (Thermo Fisher Scientific, USA).

#### 2.5. Preparation and Characterization of micelles

DTX (5 mg), BD-PEI (20 mg) and BD-PLG-PEG (20 mg) were dissolved in methanol (5 mL), then DTX-loaded BD-PEI/BD-PLG-PEG micelle (pDM) was formed by the film dispersion method. The blank BD-PEI/BD-PLG-PEG micelle (pBM) and DTX-loaded BD-PEI/BD-PEG micelle (DM) were prepared by the similar method. The DTX concentrations in pDM and DM were measured by high performance liquid chromatography (HPLC). The drug loading (DL) and encapsulation efficiency (EE) of DTX were analyzed by the following two equations:

$$DL\% = \frac{\text{Weight of the drug in micelles}}{\text{Weight of the feeding polymer and drug}} \times 100\%, \qquad (1)$$

$$EE\% = \frac{Weight\ of\ the\ drug\ in\ micelles}{Weight\ of\ the\ feeding\ drug} \times 100\%. \tag{2}$$

The morphology of pDM under different conditions was examined by transmission electron microscopy (TEM) (Tecnai F20, FEI, USA). pDM was pretreated with 50 nmol  $\rm L^{-1}$  MMP-9 or MMP-9-containing pH 5.5 acetate buffered saline (ABS) solution for 1 h before staining with phosphotungstic acid solution (1%). The mean particle sizes and zeta potential of pDM and DM with or without treatment with MMP-9 at pH 7.4, 6.8 and 5.5 were measured with a Zetasizer (Malvern, UK).

The release profile of DTX from pDM was tested in 0.1 mol  $L^{-1}$  phosphate buffered saline (PBS) at pH 7.4, PBS at pH 7.4 containing 10% FBS, PBS at pH 6.8 with/without 50 nmol  $L^{-1}$  MMP-9 and ABS at pH 5.5. The the dialysis bags containing pDM 0.5 mL (DTX concentration: 1 mg mL $^{-1}$ ) were incubated in the release media, with continuously shaking at 37 °C. The release media was replaced by fresh one at certain time points, and the DTX concentration of different samples were determined by HPLC.

#### 2.6. Cellular uptake and cytotoxicity

C6-loaded BD-PEI/BD-PLG-PEG micelle (pCM) and C6-loaded BD-PEI/BD-PEG micelle (CM) were prepared by the similar method to pDM and DM. 4 T1 cells seeded on coverslips were incubated with pCM or CM (C6 concentration:  $25 \text{ ng mL}^{-1}$ ) with or without  $50 \text{ nmol L}^{-1} \text{ MMP-9}$  pre-treating for different time at  $37 \,^{\circ}\text{C}$  in dark. Next, Hoechst 33342 and LysoTracker Red were used for staining the nuclei and lysosomes. After staining, 0.4% trypan blue was used to quench the extracellular fluorescence. 4T1 cells were washed with cold PBS and fixed with 4% paraformaldehyde. Finally, coverslips were placed onto the slide glasses and cells were observed under a laser scanning confocal microscope (LSCM, FluoView TM FV1000, Olympus, Japan).

For quantitative analysis, 4 T1 cells were treated with free DTX (DMSO solution), DM and pDM with or without 50 nmol  $L^{-1}$  MMP-9 pre-treating. The DTX concentration was 10  $\mu g \ mL^{-1}$ . After incubating for 4, 24, and 48 h,  $2\times 10^5 \ 4T1$  cells were collected, suspended with methanol and disrupted by ultrasonication. After centrifugation, the concentration of DTX in the supernatant was determined by HPLC.

The cytotoxicity was studied by the Real Time Cellular Analysis (RTCA, ACEA Biosciences Co., Ltd, China). 4 T1 cells were treated with BM, free DTX (DMSO solution), DM and pDM with or without 50 nM MMP-9 pre-treating, containing DTX of different concentrations ( $5\times10^{-3}$ ,  $10^{-2}$ ,  $5\times10^{-2}$ ,  $10^{-1}$ ,  $5\times10^{-1}$ , 1, and  $5~\mu g~mL^{-1}$ ). After incubation for 48 h, the cell viability was calculated by the RTCA software. The IC<sub>50</sub> (half maximal inhibitory concentration) values were calculated by the GraphPad Prism 6.0 software.

# 2.7. Biodistribution

DiR-loaded BD-PEI/BD-PEG micelle (DiR-M) and DiR-loaded BD-PEI/BD-PLG-PEG micelle (DiR-pM) were prepared by the same approach as DM and pDM. The 4 T1 tumor-bearing mice were randomly grouped and injected with free DiR (solution in PBS/methanol), DiR-M and DiR-pM (2 mg kg<sup>-1</sup> DiR) via tail vein. Mice were sacrificed and the tumor tissues and other major organs were obtained at 1, 4, 8 and 24 h after administration. The fluorescence intensity of DiR in each tissue was observed with small animal *in vivo* imaging instrument (IVIS, PerkinElmer, USA).

Meanwhile, 4 T1 tumor-bearing mice were randomly grouped and intravenously injected with free DTX (solution in ethanol/Cremophor EL/saline), DM and pDM (4 mg kg<sup>-1</sup> DTX). Mice were sacrificed and the main organs and tumors were harvested at 1 h, 4 h, 8 h and 24 h after administration. Each sample was homogenized in 1 mL methanol and centrifugated. The DTX concentration in the extract was determined by HPLC.

#### 2.8. Pharmacodynamics evaluation

Metastatic 4T1 tumor-bearing mouse model was founded by injection of 4T1 cells on the right mammary glands of mice. The therapy started when the tumor volumes reached approximately  $100~\mathrm{mm^3}$ . 4T1 breast cancer-bearing mice were randomized into 5 groups and administrated with saline, pBM, free DTX (solution in ethanol/Cremophor EL/saline), DM and pDM (4 mg kg $^{-1}$  DTX) through tail vein (biw × 3). Tumor volumes were measured ((major axis) × (minor axis) $^2$ /2) and recorded twice a week from the first day of treating until the end of the experiment, so were the body weights. At day 21, mice were asphyxiated to death. All the tumors and lungs were harvested and photographed. Tumors were weighed and the tumor inhibiting rate (TIR) was calculated according to Eq. (3):

$$TIR = (1 - W_{test}/W_{saline}) \times 100\%, \tag{3}$$

where,  $W_{\rm test}$  and  $W_{\rm saline}$  standed for the average tumor weight of the tested group and the saline group, respectively. The histologic sections of primary tumors were analyzed by TUNEL assays. The numbers of metastatic nodules on the lungs were counted and histologic sections of lungs were stained with hematoxylin and eosin (H&E).

#### 2.9. Biocompatibility

Healthy mice were randomly assigned into 5 groups as mentioned above. After a biw  $\times$  3 administration course, the mice were sacrificed and main organs were sectioned and stained with H&E.

#### 2.10. Statistical analysis

Every experiment was conducted at least in triplicate and the results were shown as mean values  $\pm$  SD. The difference between two groups was considered significant when  $^*P < 0.05$ , and very significant when  $^*P < 0.01$  and  $^{***}P < 0.001$ , where the p value was calculated according to the two-tailed Student's t-test and one-way analysis of variance (ANOVA) by SPSS software, and corrected by Bonferroni test for multiple comparison.

# 3. Results and discussion

# 3.1. Synthesis of the polymers

BD-PEI, BD-PEG, and BD-PLG-PEG were synthesized using Michael addition reactions (Fig. 1a). The structures of the purified polymers were confirmed by <sup>1</sup>H NMR. In the <sup>1</sup>H NMR spectrum of BD, peaks at 0.80-1.15 and 5.84-6.35 ppm, which represented the hydrogen atoms of the methyl of DPA and the double bond of acrylate, respectively, evidenced the success of polymerization (Fig. 1b). For BD-PEI, the typical peaks of the acrylate disappeared, while the signals of the methylene of PEI at 2.51-3.20 ppm increased. The <sup>1</sup>H NMR spectrum of BD-PEG was similar with BD-PEI, but the enhanced signals only appeared at 3.05-3.63 ppm, representing the methylene adjacent to the oxygen atoms of PEG. In the <sup>1</sup>H NMR spectrum of BD-PLG-PEG, the signals belonging to PLG were added or enhanced compared to BD-PEG, such as the peaks at 1.20-1.75, 3.09-3.86 and 3.99-4.75 ppm. The weight-average molecular weights  $(M_w)$  of BD-PEI, BD-PEG, and BD-PLG-PEG tested by MALDI-TOF mass spectrometer were 6.6, 13.7 and 15.0 kDa, respectively. The final yields of synthesis of BD, BD-PEI, BD-PEG and BD-PLG were 67%, 61%, 59%, and 60%, respectively. It was reported that the extent of conversion in the aza-Michael addition depended on the type of Michael acceptors, and acrylates showed high reactivity because of the good stability of the intermediate [29]. However, from the aspect of amines, the

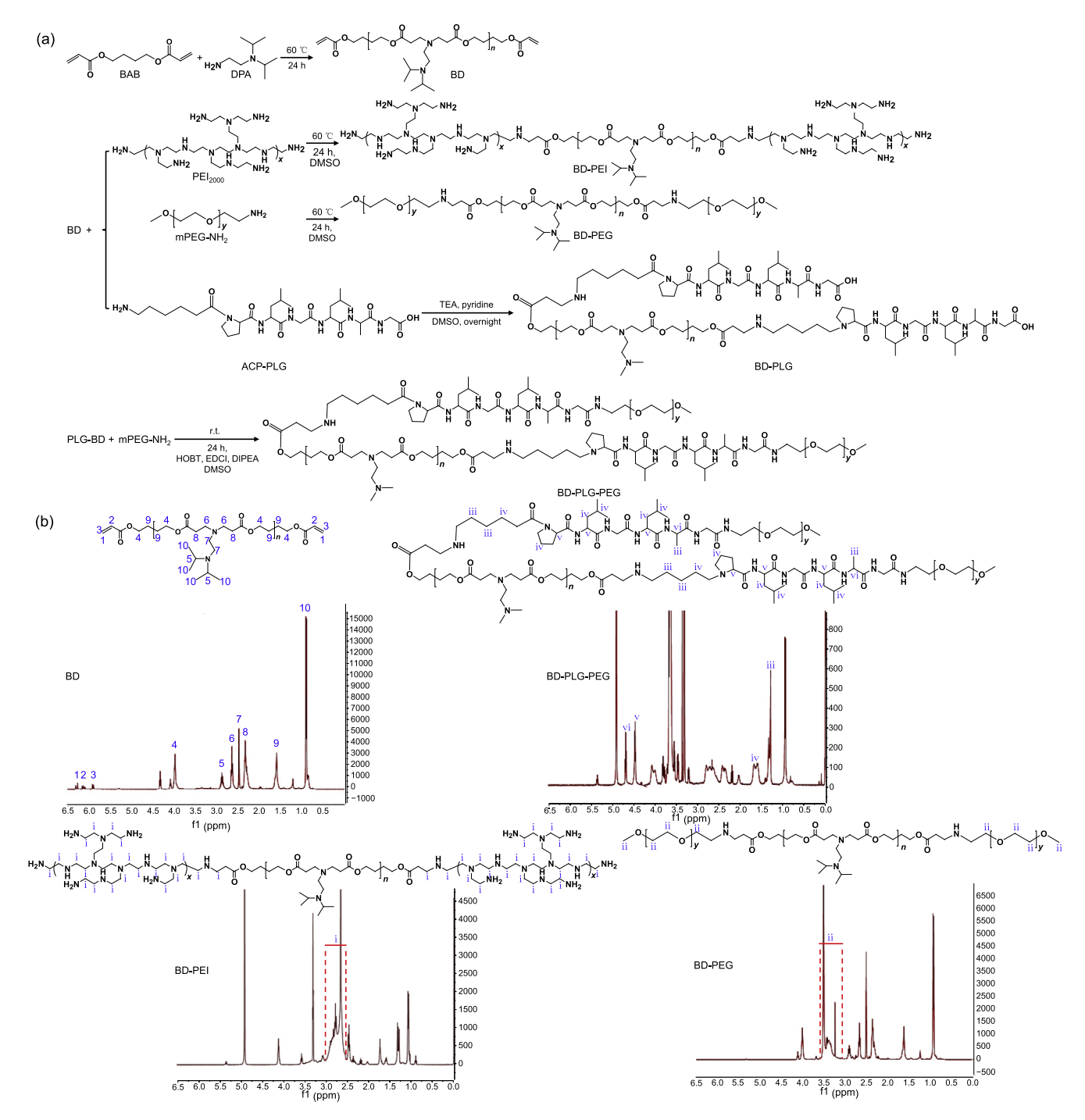


Fig. 1. (Color online) Synthesis of polymers. Synthesis flowchart (a) and <sup>1</sup>H NMR spectra (b) of BD, BD-PEI, BD-PEG, and BD-PLG-PEG.

reactivity followed the sequence of  $2^{\circ}$  amine (original) >1° amine  $\gg 2^{\circ}$  amine (formed) [30]. Therefore, the yield of the polymerization between BAB and DPA was relative low, but high yeild was obtained at the post-polymerization modification step. BD-PLG was conjugated to mPEG-NH $_2$  via the carboxyl-amino condensation reaction, with the yield of 79%. The reactants were both polymers with the  $M_{\rm w}$  no <5 kDa, so the reactivity might be affected by steric hindrance.

#### 3.2. Preparation and Characterization of pDM

The DL and EE of pDM were 9.81% and 80.54%, respectively. The TEM images showed that the untreated pDM was uniform

and spherical particle with the size of about 20 nm (Fig. 2a). The morphology change of pDM induced by MMP-9 or acid (pH 5.5) was also proved by TEM. The shell of pDM became much thinner after treated with 50 nmol L<sup>-1</sup> MMP-9, owing to the shedding of PEG corona. In the MMP-9-containing ABS solution (pH 5.5), pDM presented incomplete and degradative structure but not the previous spherical shape. The TEM results substantiated that pDM was sensitive to both acid and MMP-9. The particle size and zeta potential of pDM measured by dynamic light scattering (DLS) were consistent with TEM images. 1 h post incubation with MMP-9, the mean particle size of pDM decreased from 24.36 nm (polydispersity (PDI) 0.14) to 15.68 nm and the zeta potential increased from -1.44 to 2.29 mV, suggesting that

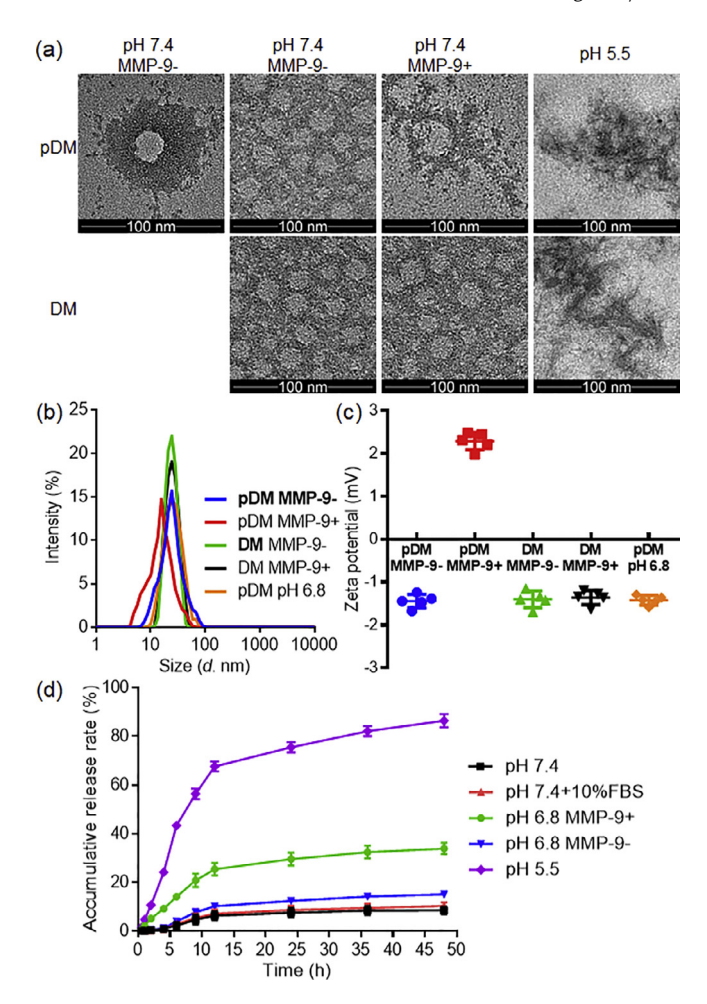


**Fig. 2.** Characterization of pDM and DM. (a) TEM images of pDM and DM with different treatment. Scale bars: 100 nm. Particle sizes (b) and zeta potential (c) of pDM and DM with/without MMP-9 treatment at pH 7.4 or 6.8 determined by DLS. (d) Time-dependent cumulative release of DTX from pDM in different media.

the cationic charges of PEI were exposed after the removing of PEG by MMP-9 (Fig. 2b and c). In addition, DM, with the mean particle size of 23.95 nm (PDI 0.18) and zeta potential of -1.40 mV, did not show these variations under the action of MMP-9, thus could be used as the non-MMP-9-sensitive control of pDM in the following studies. The size and surface charge of pDM at pH 6.8 hardly changed, with the mean particle size of 23.56 nm and the zeta potential of -1.42 mV. However, these data could not be detected at pH 5.5, due to the dissociation of pDM in strongly acidic conditions.

According to the drug release profiles, neutral and slightly acidic pH barely induced drug release from pDM, as <20% DTX was released within 48 h in pH 7.4 PBS, pH 7.4 PBS containing 10% fetal bovine serum (FBS), and pH 6.8 PBS, which mimics conditions of the tissue fluid/blood circulation (pH 7.4/pH 7.4 + 10% FBS) and the extracellular space of the tumor tissues (pH 6.8) (Fig. 2d). The drug release in pH 6.8 PBS + MMP-9 was faster than that without MMP-9, which might be because pDM was destabilized after losing the PEG shell. However, more than 65% of DTX still remained in the micelles, meaning that DTX would not be pre-released in the extracellular space at tumor tissues. In the pH 5.5 medium, the drug release rate was more than 80% at 48 h, which was a sign of ample and prompt intracellular DTX release in the endo/lysosomes of tumor cells [31].

#### 3.3. Cellular uptake and cytotoxicity

The hydrophobic fluorescent dve C6 was selected to replace DTX to observe the cellular uptake and intracellular transportation of drugs delivered by the micelles by LSCM. Although 4T1 is a MMP-9-overexpressing cell line, MMP-9 is synthesized and secreted as the proenzyme and needs activating by other molecules in the tumor microenvironment [32]. So the local concentration of active MMP-9 in the 4T1 tumor tissue in vivo is much higher than that in the cell culture medium in vitro. Therefore, to simulate the conditions in vivo, there were one CM group and one pCM group being pretreated with active MMP-9 before it was incubated with cells. After 4T1 cells were incubated with MMP-9 treated pCM for only 1 h, strong green fluorescence was detected in the cytoplasm. In addition, the fluorescen t intensity got stronger in the process of internalization, which indicated that the BD-PEI/BD-PLG-PEG micelle was able to deliver hydrophobic drugs to the cytoplasm of cancer cells efficiently with the assistance of MMP-9 (Fig. 3a). However, when pCM had not been treated with MMP-9, its fluorescence signal in 4T1 cells was quite weak all the time. The cellular uptake rate of CM was rather low, whether pre-treated with MMP-9 or not.

Similarly, in the quantitative analysis, after incubation for 4 h, the intracellular DTX concentration of the DM + MMP-9 group was no higher than that of the DM alone group, which was a little lower than the free DTX group and approximately equal to the pDM alone group (Fig. 3b). The DTX concetration of the pDM + MMP-9 group was 1.9 times of that without MMP-9. It probably resulted from the abscission of PEG from pDM in the action of MMP-9. After this process, the surface charge of pDM converted to positive, which enhanced the cell uptake efficiency [33]. When the incubation time was expanded to 24 and 48 h, the intracellular DTX concentration steeply decreased. Most cells of the pDM + MMP-9 group were dead, but in the living cells, this group still had higher DTX content than other groups.

The anti-proliferation efficacy of the DTX-containing formulations in vitro was investigated by the RTCA equipment (Fig. 3c). pBM with the polymer concentrations up to 40  $\mu$ g mL<sup>-1</sup> showed negligible toxicity in 4T1 cells, suggesting that BD-PEI and BD-PLG-PEG were biocompatible when playinge role as the drug carrier. Compared to free DTX (IC<sub>50</sub> 0.98  $\mu$ g mL<sup>-1</sup>), the IC<sub>50</sub> value of DM (4.27  $\mu$ g mL<sup>-1</sup>) after 48 h incubation was even higher and its combination with MMP-9 did not work to increase cytotoxicity (IC<sub>50</sub> 4.30  $\mu$ g mL<sup>-1</sup>). The enhancement of cytotoxicity of pDM alone was very limited compared to DM, with the IC<sub>50</sub> value of 3.95  $\mu$ g mL<sup>-1</sup>, but pDM pretreated by MMP-9 increased the cytotoxicity by 3.19 times compared with free DTX. The enhanced cytotoxicity was likely attributed to the higher intracellular DTX concentration mediated by pDM.

# 3.4. Biodistribution

In the tumor-targeting delivery of drugs for cancer therapy, enough biodistribution of drugs in the tumor site is essential [34]. Here the biodistribution of DTX delivered as free state, in DM and in pDM were investigated. The infrared fluorescence dye DiR was used to replace DTX for qualitative observation (Fig. 4a). Within 24 h post administration, free DiR mainly distributed in important organs of drug metabolism, like liver, spleen and kidney [35]. The fluorescence intensity in tumors was relatively low, indicating that free drugs did not own targeting capacity towards tumors. Though compared with free DiR, the intratumoral accumulation of DiR delivered by DiR-M was increased and prolonged, which could be detected at 24 h after injection, the fluorescence was still weak. Perhaps PEG not only prolonged the circulating

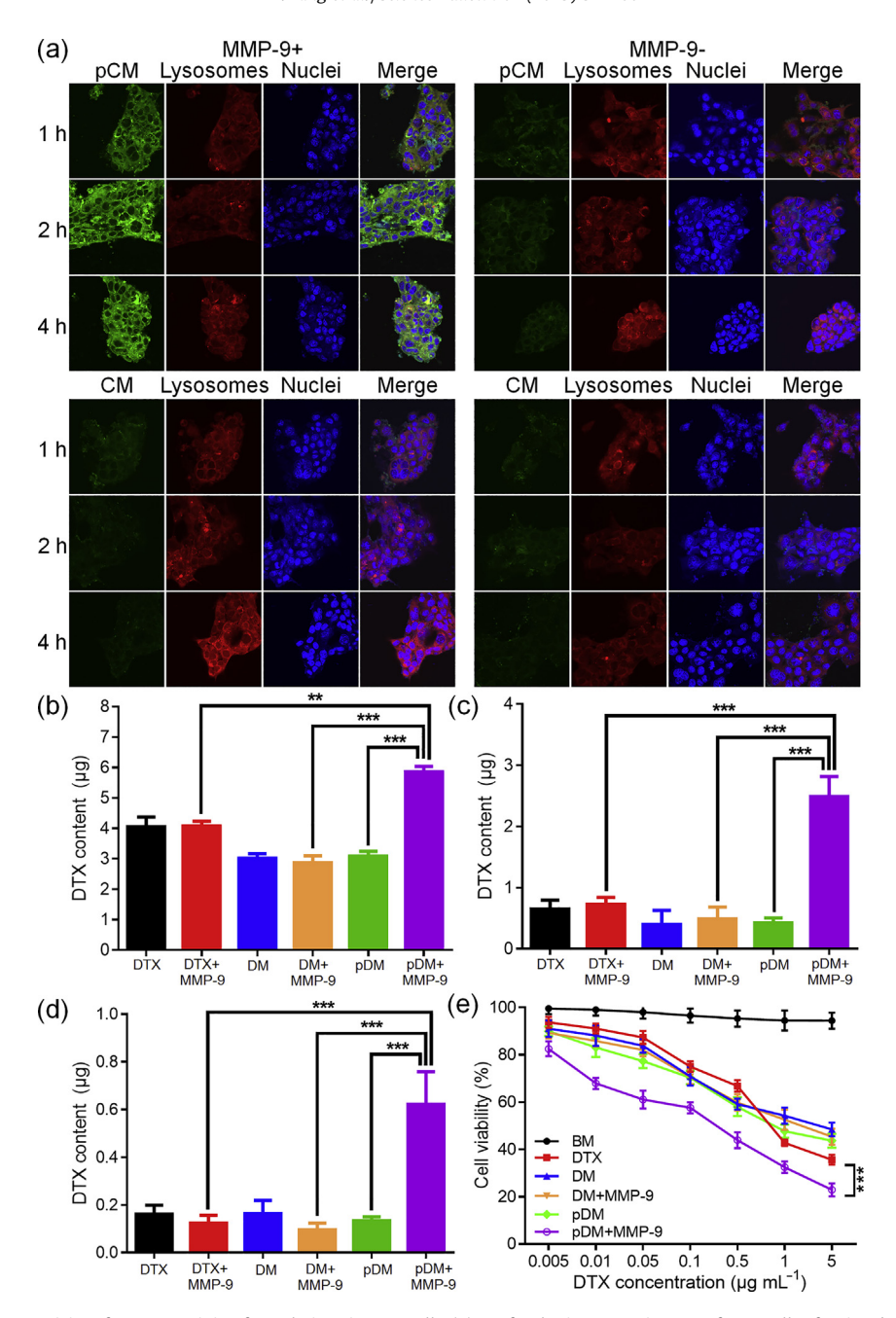
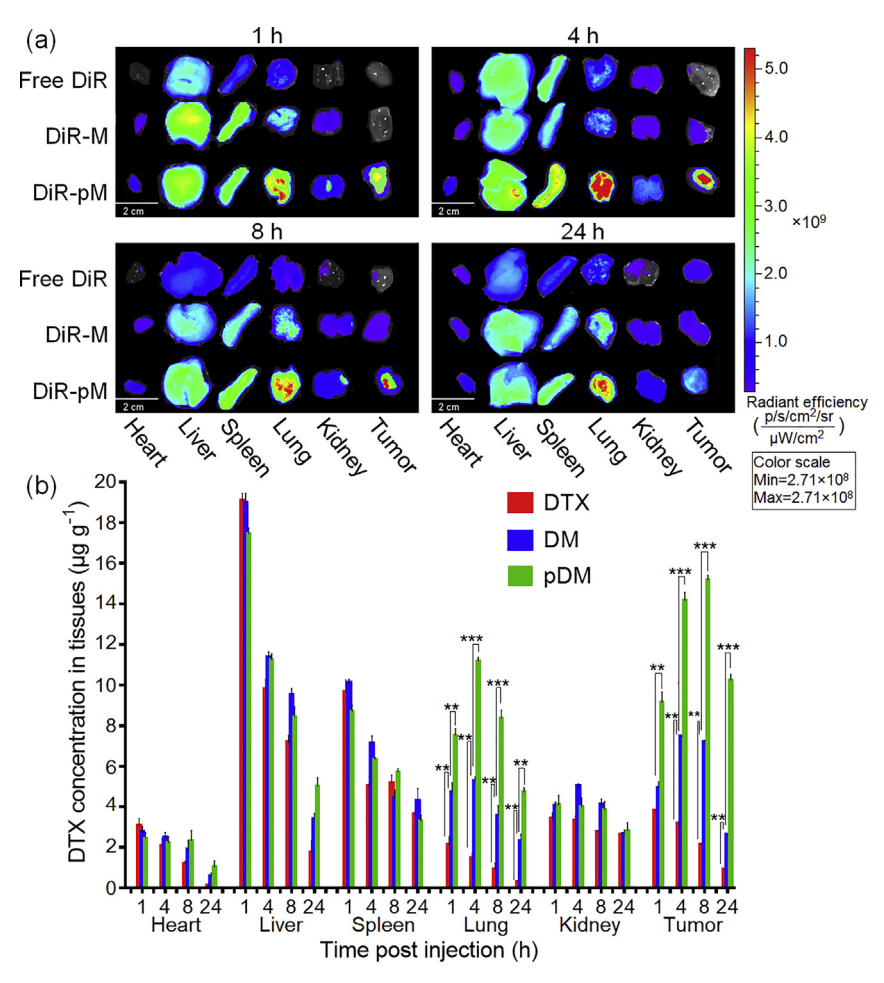


Fig. 3. Cellular uptake and cytotoxicity of DTX-containing formulations in 4 T1 cells. (a) Confocal microscopy images of 4 T1 cells after incubated for 1, 2 and 4 h with pCM and CM with/without MMP-9 treatment. DTX was replaced with C6 (green). Lysosomes and nuclei were stained with LysoTracker Red (red) and Hoechst 33342 (blue), respectively (magnification:  $60 \times$ ). Intracellular DTX content in  $2 \times 10^5$  4T1 cells after treatment for 4 h (b), 24 h (c), and 48 h (d) with free DTX, DM and pDM with/without MMP-9 treatment. (e) Viability of 4T1 cells after incubated for 48 h with BM, free DTX, DM and pDM at different concentrations with/without MMP-9 treatment. "P < 0.001, and "P < 0.001.

time of micelles but also impeded the cellular uptake. So most DiR-M could not be internalized by tumor cells but taken away by bloodstream. Comparatively, the intratumoral accumulation of DiR delivered by DiR-pM was obviously increased, because the shedding of PEG in the MMP-9-overexpressing environment of tumor tissues would promote the endocytosis of micelles in 4 T1 cells. Unexpectedly, the accumulation of DiR-pM in liver, kidney and lung was also increased. This part of micelles might have arrived at tumor tissues and removed PEG, but flowed back to the circulation before tumor cells captured them. The positive charges led to their distribution in mononuclear-phagocyte system organs.

Concordant with the in vivo imaging, the quantitative analysis showed that the intratumoral DTX accumulation of the pDM group was increased by at least two times compared with free DTX and DM (Fig. 4b). The accumulation of DTX in tumor cells also profited from the design of pDM, that two different amphiphilic polymers were contained in the system. If only BD-PLG-PEG was used to construct the drug carrier, it would dissociate and release drugs at the extracellular space of tumor tissues. Free drugs would be easier to flow back to circulation than in the form of being encapsulated in a nanocarrier, since the latter could exploit the EPR effect to be detained at the tumor tissues. So the cationic BD-PEI was added in the system, to maintain the nano-structure after taking off



**Fig. 4.** Biodistribution of different formulations. (a) Fluorescence images of tumors and organs of mice at 1, 4, 8, and 24 h after intravenously administrated with free DIR, DiR-M and DiR-pM. (b) The amounts of PTX in tumors and organs at 1, 4, 8, and 24 h after intravenously administrated with free DTX, DM and pDM. "P < 0.01, and "P < 0.001."

PEG, and to promote the internalization by tumor cells. These results demonstrated that pDM was an efficient vehicle to deliver DTX into tumor cells in vivo.

# 3.5. In vivo pharmacodynamics and biocompatibility

The tumor volumes of 4T1 tumor-bearing mice administrated with various formulations were monitored for evaluating the antitumor effects. Within the 21-d therapy period, the saline and pBM groups showed similar tumor growing profiles, indicating that the blank carrier had no anti-tumor activity (Fig. 5a and b). Free DTX showed limited tumor-suppressing ability due to low intratumoral drug concentrations, whose tumor inhibiting rate (TIR) was only 25.3%. But DTX caused severe loss of body weights due to systemic side effects (Fig. 5c). DM and pDM presented improved inhibition efficacy on tumor growth, with the TIR of 33.4% and 88.1%, respectively, while keeping the body weights at a stable level. Hence, delivering DTX in the form of micelle were able to promote the anti-tumor effect due to EPR effect of solid tumors. The antitumor effect of pDM was dramatically superior to that of DM, suggesting that the sensitivity of pDM to tumor environment benefited the chemotherapy with DTX. Meanwhile, throughout the therapy period, the early dose killed most tumor cells and expanded the extracellular space in tumor tissues, which improved the penetration of micelles in the later doses [36]. The result of the TUNEL staining assay was in accordance with the tumor volumes (Fig. 5d). There was rarely apoptosis in tumor cells of the saline and pBM groups. The free DTX group showed slight apoptosis with weak green fluorescence. For DM and pDM groups, most tumors cells were apoptotic, of the two pDM was more obvious. The dUTP-positive rate of the saline, pBM, DTX, DM and pDM groups were 0.13%, 0.78%, 24.87%, 43.31%, and 77.59%, respectively.

Breast cancer patients always die from tumor metastasis in distant organs, the most common one of which is the lung [37]. For curing breast cancer, it is essential to control over the lung metastases formation. The saline and pBM groups had 34 and 33 metastatic nodules on average, respectively (Fig. 5e). The surface of lungs of these two groups were spotted with metastases (Fig. 5f). The tumor burdens, presented as high density variation on the H&E-stained lung sections, covered most area (Fig. 5g). The average numbers of metastatic nodules of free DTX and DM groups decreased to 22.4 and 11.2, respectively. The lung sections showed smaller tumor burden area than the saline group. Comparing with the saline group, the lung metastases of the pDM group decreased by 95.88%, with only one or even no metastatic nodule on each lung. The numbers of the lung metastasis foci were positively correlated with the primary tumor volumes, indicating that the inhibition of lung metastasis was probably influenced by the development degree of primary tumors [38]. On the other hand, the obvious lung metastasis inhibiting effect of pDM might also benefit from its high intrapulmonary accumulation, which directly destroy the cancer cells transferred to lungs [39]. These results indicated that pDM, owning good tumor-targeting ability, could effectively suppress tumor growth and adequately reduce pulmonary metastasis, thus would be an excellent DTX delivery platform for breast cancer therapy.

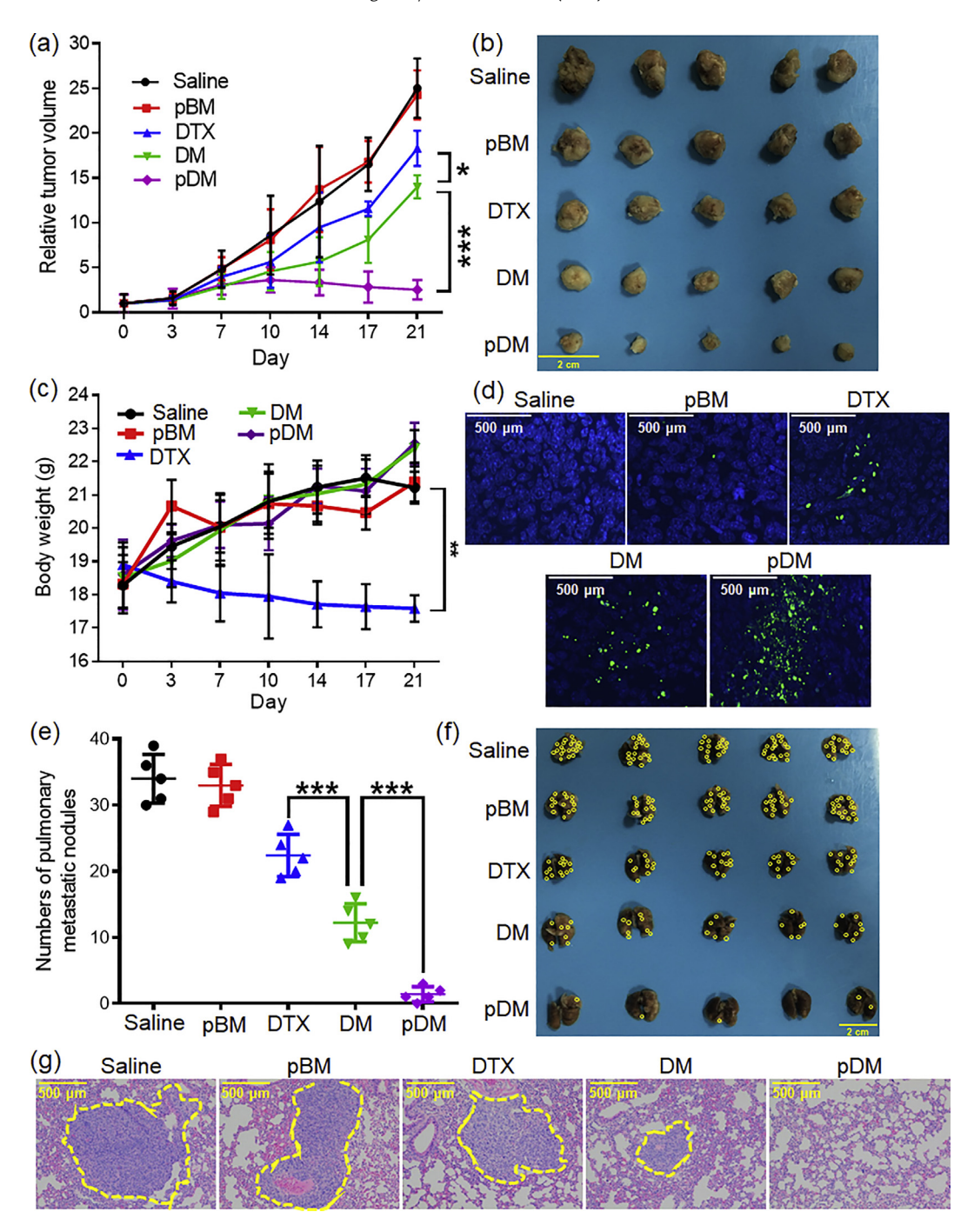


**Fig. 5.** In vivo anti-tumor and anti-metastasis efficiency in mice bearing 4T1 tumors treated with a schedule of multiple doses. (a) The curves of tumor volumes variation. (b) The images of tumors at the end of the experiment. (c) The variation curves of body weights. (d) The TUNEL examination of tumor sections at the end of the experiment. (e) Numbers of the pulmonary metastatic nodules. (f) Images of the lungs at the end of the experiment (yellow circles labeling the lungs pointed out the metastatic nodules). (g) H&E staining of the lung sections at the end of the experiment. Data were given as mean ± SD (n = 5). \*P < 0.05, \*\*P < 0.01, and \*\*\*P < 0.001.

The H&E-stained major organ sections did not show obvious pathological variation, illustrating that DM and pDM showed good biocompatibility (Fig. 6).

# 4. Conclusions

In summary, the DTX-loaded micelle (pDM) based on a pH-sensitive polymer, BD-PEI, and an MMP-9-sensitive polymer, BD-PLG-PEG, were designed and constructed. The PEG coating would

be stripped under the action of MMP-9 when pDM arrived at tumor sites in 4T1 tumor-bearing mice, which resulted in enhanced DTX accumulation inside 4T1 cells. Then DTX could be rapidly released in an acid-triggered manner. pDM exhibited powerful ability of suppressing the growth and metastasis of tumor in vitro and in vivo. Good biocompatibility of pDM was proved via the histological analysis of the main organs. The results demonstrated that pDM owned the potential to be applied as a tumor-microenviron ment-responsive DTX delivery platform for effective treatment of metastatic breast cancer.

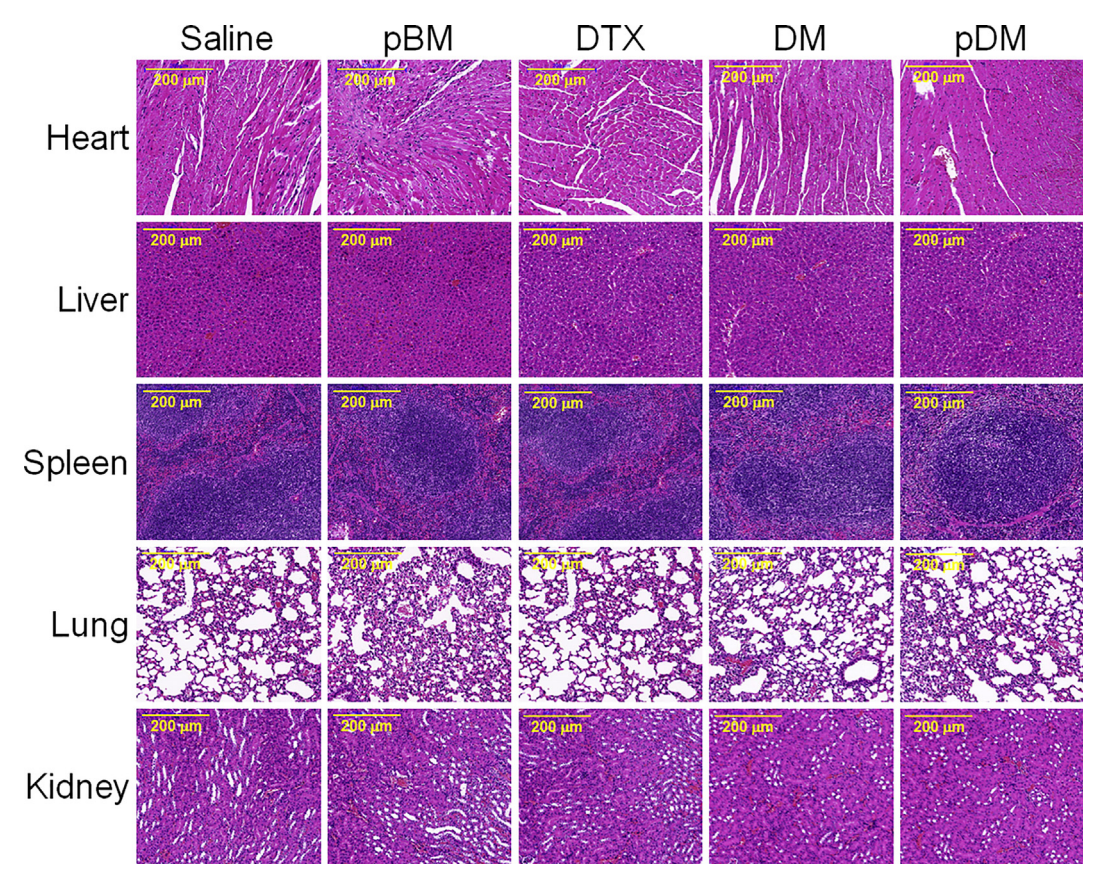


Fig. 6. Tissue sections stained with hematoxylin and eosin from healthy mice received a schedule of multiple doses.

# **Conflict of interest**

The authors declare that they have no conflict of interest.

# Acknowledgements

This work was supported by the National Natural Science Foundation of China (81871471, 81630052, 81690265, and 81521005), Key Scientific Research Program of Chinese Academy of Sciences (QYZDJSSW-SMC020), and the Youth Innovation Promotion Association of Chinese Academy of Sciences (2015226). The authors are extremely grateful to National Centre for Protein Science Shanghai for their instrument support and technical assistance.

#### **Author contributions**

Lang T, Dong X and Yin Q designed the project; Lang T, Zheng Z, Dong X, and Liu Y performed the experiments; Lang T, Dong X, Yin Q, and Li Y analyzed the data and wrote the manuscript.

# Appendix A. Supplementary data

Supplementary data to this article can be found online at https://doi.org/10.1016/j.scib.2018.12.025.

# References

- [1] Siegel RL, Miller KD, Jemal A. Cancer statistics, 2017. Ca-Cancer J Clin 2017;67:7–30.
- [2] Chen DH, Sun YT, Wei YK, et al. LIFR is a breast cancer metastasis suppressor upstream of the Hippo-YAP pathway and a prognostic marker. Nat Med 2012;18:1511–5.

- [3] He B, Hu HY, Tan T, et al. IR-780-loaded polymeric micelles enhance the efficacy of photothermal therapy in treating breast cancer lymphatic metastasis in mice. Acta Pharmacol Sin 2018;39:132–9.
- [4] Gligorov J, Richard S. Weekly paclitaxel-still preferred first-line taxane for mBC. Nat Rev Clin Oncol 2015;12:508–25.
- [5] Arnedos M, Vicier C, Loi S, et al. Precision medicine for metastatic breast cancer-limitations and solutions. Nat Rev Clin Oncol 2015;12:693–704.
- [6] Guo MY, Zhou GQ, Liu Z, et al. Direct site-specific treatment of skin cancer using doxorubicin-loaded nanofibrous membranes. Sci Bull 2018;63:92–100.
- [7] Sagnella SM, McCarroll JA, Kavallaris M. Drug delivery: beyond active tumour targeting. Nanomed Nanotechnol 2014;10:1131–7.
- [8] Jahangirian H, Lemraski EG, Webster TJ, et al. A review of drug delivery systems based on nanotechnology and green chemistry: green nanomedicine. Int J Nanomed 2017;12:2957–77.
- [9] Tong CY, Zhang XZ, Fan JL, et al. PEGylated mBPEI-rGO nanocomposites facilitate hepotocarcinoma treatment combining photothermal therapy and chemotherapy. Sci Bull 2018;63:935–46.
- [10] Kobayashi H, Watanabe R, Choyke PL. Improving conventional enhanced permeability and retention (EPR) effects; what is the appropriate target? Theranostics 2014;4:81–9.
- [11] Hua X, Li FY, Noor N, et al. Platinum drugs: from Pt(II) compounds, Pt(IV) prodrugs, to Pt nanocrystals/nanoclusters. Sci Bull 2017;62:589–96.
- [12] Shao SQ, Zhou Q, Si JX, et al. A non-cytotoxic dendrimer with innate and potent anticancer and anti-metastatic activities. Nat Biomed Eng 2017;1:745-57.
- [13] Rajora AK, Ravishankar D, Osborn HMI, et al. Impact of the enhanced permeability and retention (EPR) effect and cathepsins levels on the activity of polymer-drug conjugates. Polymers 2014;6:2186–220.
- [14] Feng LZ, Dong ZL, Tao DL, et al. The acidic tumor microenvironment: a target for smart cancer nano-theranostics. Natl Sci Rev 2018;5:269–86.
- [15] Liang XL, Li YY, Li XD, et al. PEGylated polypyrrole nanoparticles conjugating gadolinium chelates for dual-modal MRI/photoacoustic imaging guided photothermal therapy of cancer. Adv Funct Mater 2015;25:1451–62.
- [16] Murali K, Kenesei K, Li Y, et al. Uptake and bio-reactivity of polystyrene nanoparticles is affected by surface modifications, ageing and LPS adsorption: in vitro studies on neural tissue cells. Nanoscale 2015;7:4199–210.
- [17] Huang D, Wang YQ, Yang F, et al. Charge-reversible and pH-responsive biodegradable micelles and vesicles from linear-dendritic supramolecular amphiphiles for anticancer drug delivery. Polym Chem 2017;8:6675–87.
- [18] Liu J, Huang YR, Kumar A, et al. pH-Sensitive nano-systems for drug delivery in cancer therapy. Biotechnol Adv 2014;32:693–710.
- [19] Yin XL, Chi YY, Guo CY, et al. Chitooligosaccharides modified reductionsensitive liposomes: enhanced cytoplasmic drug delivery and osteosarcomastumor inhibition in animal models. Pharm Res 2017;34:2172–84.

- [20] Liu F, Li X, Zhang LY, et al. Stimuli-Responsive nanocarriers for drug delivery to the central nervous system. Curr Nanosci 2016;12:4–17.
- [21] Mura S, Nicolas J, Couvreur P. Stimuli-responsive nanocarriers for drug delivery. Nat Mater 2013;12:991–1003.
- [22] Lang TQ, Ran W, Dong XY, et al. Tumor cells-selective bionic nanodevice exploiting heparanase combats metastatic breast cancer. Adv Funct Mater 2018;28:1707289.
- [23] Wen R, Lv XY, Yang T, et al. Albumin nanoreactor-templated synthesis of Gd<sub>2</sub>O<sub>3</sub>/CuS hybrid nanodots for cancer theranostics. Sci China Mater 2017:60:554–62.
- [24] Veiman KL, Kunnapuu K, Lehto T, et al. PEG shielded MMP sensitive CPPs for efficient and tumor specific gene delivery in vivo. J Control Release 2015;209:238–47.
- [25] Isaacson KJ, Jensen MM, Subrahmanyam NB, et al. Matrix-metalloproteinases as targets for controlled delivery in cancer: an analysis of upregulation and expression. J Control Release 2017;259:62–75.
- [26] Wang HX, Yang XZ, Sun CY, et al. Matrix metalloproteinase 2-responsive micelle for siRNA delivery. Biomaterials 2014;35:7622–34.
- [27] Lei Z, Wang JQ, Lv P, et al. Biomimetic synthesis of nanovesicles for targeted drug delivery. Sci Bull 2018;63:663–5.
- [28] Hama S, Itakura S, Nakai M, et al. Overcoming the polyethylene glycol dilemma via pathological environment-sensitive change of the surface property of nanoparticles for cellular entry. J Control Release 2015;206:67–74.
- [29] Narayanan A, Maiti B, De P. Exploring the post-polymerization modification of side-chain amino acid containing polymers via Michael addition reactions. React Funct Polym 2015;91–92:35–42.
- [30] Cheng WR, Wu DC, Liu Y. Michael addition polymerization of trifunctional amine and acrylic monomer: a versatile platform for development of biomaterials. Biomacromolecules 2016;17:3115–26.
- [31] Wang X, Yang YY, Zhuang YP, et al. Fabrication of pH-responsive nanoparticles with an AIE feature for imaging intracellular drug delivery. Biomacromolecules 2016:17:2920-9.
- [32] Cathcart J, Pulkoski-Gross A, Cao J. Targeting matrix metalloproteinases in cancer: bringing new life to old ideas. Genes Dis 2015;2:26–34.
- [33] Liu X, Xiang JJ, Zhu DC, et al. Fusogenic reactive oxygen species triggered charge-reversal vector for effective gene delivery. Adv Mater 2016;28:1743–52.
- [34] Kunjachan S, Pola R, Gremse F, et al. Passive versus active tumor targeting using RGD- and NGR-modified polymeric nanomedicines. Nano Lett 2014:14:972-81.
- [35] Bao YJ, Jin Y, Chivukula P, et al. Effect of PEGylation on biodistribution and gene silencing of siRNA/lipid nanoparticle complexes. Pharm Res 2013;30:342–51.
- [36] Luan X, Guan YY, Lovell JF, et al. Tumor priming using metronomic chemotherapy with neovasculature-targeted, nanoparticulate paclitaxel. Biomaterials 2016;95:60–73.
- [37] Conde J, Bao CC, Tan YQ, et al. Dual targeted immunotherapy via in vivo delivery of biohybrid RNAi-peptide nanoparticles to tumor-associated macrophages and cancer cells. Adv Funct Mater 2015;25:4183–94.
- [38] Zhang Y, Yang PY, Sun T, et al. miR-126 and miR-126\*repress recruitment of mesenchymal stem cells and inflammatory monocytes to inhibit breast cancer metastasis. Nat Cell Biol 2013;15:284–94.
- [39] Albers AE, Grabow R, Qian X, et al. Efficacy and toxicity of docetaxel combination chemotherapy for advanced squamous cell cancer of the head and neck. Mol Clin Oncol 2017;7:151–7.



Tianqun Lang obtained his B.S. degree in pharmacy from Sun Yat-sen University in 2015. He has been studying at the Shanghai Institute of Materia Medica, Chinese Academy of Sciences, for his Ph.D. in pharmaceutics since 2015. He works on the design and construction of nano-drug delivery systems for metastatic breast cancer-targeting therapy under the guidance of Prof. Yaping Li.



Xinyue Dong studied at the Shanghai Institute of Material Medica, Chinese Academy of Sciences under the guidance of Prof. Yaping Li from 2015 to 2017 as a joint training graduate student from University of Science and Technology of China, and obtained her M.S. degree in chemical engineering in 2017. She works on the design and construction of tumor-targeting nanodrug delivery systems and plasmonic nanomaterials for biomedical applications.



Qi Yin got her Ph.D. from the Center of Pharmaceutics, Shanghai Institute of Materia Medica, Chinese Academy of Sciences, and is now working as an associate professor. She has long been committed to the research and development of nanotechnology-based drug delivery systems and has obtained important results in constructing new nano drug delivery systems that improve the efficacy of chemotherapy for reversing multidrug resistance and treating metastatic breast cancer.



Yaping Li is a principal investigator and director in Center of Pharmaceutics, Shanghai Institute of Materia Medica, Chinese Academy of Sciences. He has made a series of contributions to the basic research and clinical translation of targeted drug delivery systems, including the design, construction, and mechanistic study of novel nanosized drug delivery stems with higher efficacy and low toxicity for the treatment of metastatic and multidrug resistant cancer.